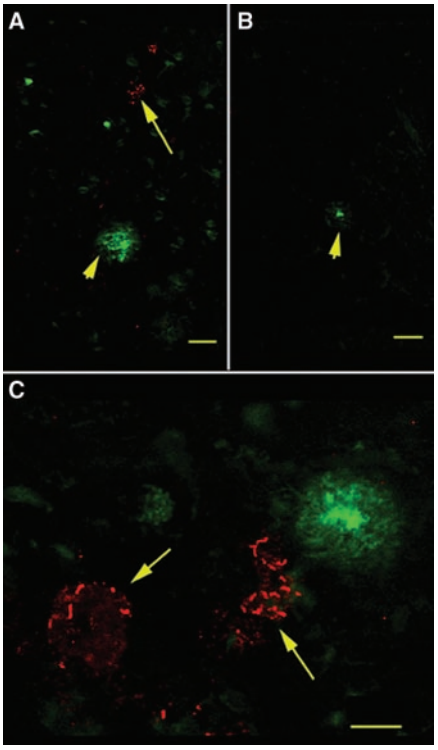

Fig. 3. Confocal immunofluorescence micrographs of human brain tissue. Sections from the entorhinal cortex of (**A**) an AD brain and (**B**) an age-matched control case were immunostained with oligomer-specific antibody (red) (arrows) and counterstained with thioflavin-S (green). Note the single thioflavin-S–positive plaque in the control case (arrowhead) and lack of oligomer-specific antibody fluorescence. (**C**) Oligomer-specific antibody positive deposits were observed in the AD case. When such deposits were found in association with a thioflavin-S–positive plaque, higher magnification and a Z-series indicated that the two deposits were spatially segregated. Scale bars, 20 μm.

have a conformation that is distinct from that of soluble monomers, low-MW oligomers, and fibrils. The fact that this epitope is common to amyloids of widely varying primary sequence further indicates that the epitope is formed from a specific conformation of the polypeptide backbone and is largely independent of the amino acid side chains in this region. A similar type of antibody specificity was recently reported by Wetzel and co-workers (*18*), but this antibody is specific for all types of amyloid fibrils and does not recognize soluble oligomers. Stefani and co-workers (*11*) have recently reported that soluble oligomers formed from non–disease-related proteins are inherently cytoxic, suggesting that they may have a common structure and function. Because the oligomer-specific antibody neutralizes the toxicity of oligomeric forms of all amyloids tested, they share a common structure, and they have a common mechanism of pathogenesis that is intimately associated with this common structure. This mechanistic commonality represents an important advance in our understanding of the mechanism of amyloid pathogenesis because it argues against a specific mechanism for one type of amyloid that is untenable for all of them. Because some amyloids, like Aβ, are in the extracellular space or the lumenal contents of the secretory and endocytic pathways, whereas other amyloids, like α-synuclein, reside in the cytosolic compartment, components that reside exclusively in either compartment are excluded as primary targets. In contrast, a common mechanism argues in favor of components that are accessible from both extracellular and cytosolic compartment, such as cell membranes as primary targets of amyloid pathogenesis.

References and Notes

1. J. Hardy, D. J. Selkoe, *Science* **297**, 353 (2002).
2. D. M. Hartley *et al.*, *J. Neurosci.* **19**, 8876 (1999).
3. M. P. Lambert *et al.*, *Proc. Natl. Acad. Sci. U.S.A.* **95**, 6448 (1998).
4. B. Soreghan, J. Kosmoski, C. Glabe, *J. Biol. Chem.* **269**, 28551 (1994).
5. L. O. Tjernberg *et al.*, *Chem. Biol.* **6**, 53 (1999).
6. H. LeVine, 3rd, *Arch. Biochem. Biophys.* **404**, 106 (2002).
7. M. Pitschke, R. Prior, M. Haupt, D. Riesner, *Nature Med.* **4**, 832 (1998).
8. Y. M. Kuo *et al.*, *J. Biol. Chem.* **271**, 4077 (1996).
9. C. A. McLean *et al.*, *Ann. Neurol.* **46**, 860 (1999).
10. L. F. Lue *et al.*, *Am. J. Pathol.* **155**, 853 (1999).
11. M. Bucciantini *et al.*, *Nature* **416**, 507. (2002).
12. J. D. Harper, S. S. Wong, C. M. Lieber, P. T. Lansbury Jr., *Biochemistry* **38**, 8972 (1999).
13. K. A. Conway, J. D. Harper, P. T. Lansbury Jr., *Biochemistry* **39**, 2552 (2000).
14. C. Goldsbury, J. Kistler, U. Aebi, T. Arvinte, G. J. Cooper, *J. Mol. Biol.* **285**, 33 (1999).
15. T. R. Serio *et al.*, *Science* **289**, 1317 (2000).
16. O. M. El-Agnaf, S. Nagala, B. P. Patel, B. M. Austen, *J. Mol. Biol.* **310**, 157 (2001).
17. H. A. Lashuel, D. Hartley, B. M. Petre, T. Walz, P. T. Lansbury Jr., *Nature* **418**, 291. (2002).
18. B. O'Nuallain, R. Wetzel, *Proc. Natl. Acad. Sci. U.S.A.* **99**, 1485. (2002).
19. This work was supported by NIH grants NS31230, AG00538, and AG16573 and by a grant from the Larry L. Hillblom foundation. We are grateful to D. A. Brant, Department of Chemistry, University of California, Irvine, for his support; R. Wetzel for providing the polyglutamine peptide; F. Saroza for technical assistance; and R. Langen for providing α-synuclein. R.K. thanks K. Sweimeh and Y. Al-Abed for helpful discussions.

Supporting Online Material

www.sciencemag.org/cgi/content/full/300/5618/486/DC1
Materials and Methods
SOM Text
Figs. S1 to S4
References
Movie S1

16 October 2002; accepted 21 March 2003

Induction of Tumors in Mice by Genomic Hypomethylation

François Gaudet,[1,2,3] J. Graeme Hodgson,[4] Amir Eden,[1] Laurie Jackson-Grusby,[1] Jessica Dausman,[1] Joe W. Gray,[4] Heinrich Leonhardt,[2,3] Rudolf Jaenisch[1]*

Genome-wide DNA hypomethylation occurs in many human cancers, but whether this epigenetic change is a cause or consequence of tumorigenesis has been unclear. To explore this phenomenon, we generated mice carrying a hypomorphic DNA methyltransferase 1 (*Dnmt1*) allele, which reduces Dnmt1 expression to 10% of wild-type levels and results in substantial genome-wide hypomethylation in all tissues. The mutant mice were runted at birth, and at 4 to 8 months of age they developed aggressive T cell lymphomas that displayed a high frequency of chromosome 15 trisomy. These results indicate that DNA hypomethylation plays a causal role in tumor formation, possibly by promoting chromosomal instability.

Human cancer cells often display abnormal patterns of DNA methylation. The role of aberrant hypermethylation in the silencing of tumor suppressor genes is now well documented (*1*). In contrast, the role of aberrant hypomethylation—which is observed in a wide variety of tumors (*2*–*5*), often together with regional hypermethylation—has remained unclear.

To investigate whether DNA hypomethylation has a causal role in tumor formation, we generated mice with highly reduced levels of Dnmt1, the enzyme that maintains DNA methylation patterns in somatic cells (*6*). Because mice homozygous for a Dnmt1 null allele ($Dnmt1^{c/c}$) die during gestation (*7, 8*), we combined a hypomorphic allele [$Dnmt1^{chip}$ (*9*)] with a null allele to generate $Dnmt1^{chip/c}$ (referred to here as $Dnmt1^{chip/-}$) compound heterozygotes with a substantially reduced level of genome-wide DNA methyl-

[1]Whitehead Institute for Biomedical Research and Department of Biology, Massachusetts Institute of Technology, Cambridge, MA 02142, USA. [2]Ludwig Maximilians University, Department of Biology II, 80336 Munich, Germany. [3]Max Delbrück Center for Molecular Medicine, 13125 Berlin, Germany. [4]Department of Laboratory Medicine and UCSF Comprehensive Cancer Center, University of California, 2340 Sutter Street, San Francisco, CA 94143, USA.

*To whom correspondence should be addressed. E-mail: jaenisch@wi.mit.edu

ation. *Dnmt1*$^{chip/-}$ embryonic stem (ES) cells expressed 10% of wild-type levels (Fig. 1A). To test whether the reduced Dnmt1 expression affected DNA methylation in vivo, we generated mice carrying the different *Dnmt1* alleles and determined their global methylation levels with the use of a probe for endogenous retroviral A type particles (IAPs) (Fig. 1, B and D) (*10*) and centromeric repeats (Fig. 1C). Southern blot analysis of embryonic fibroblasts and adult tissues showed that the DNA from compound heterozygotes was hypomethylated relative to the DNA from *Dnmt1*$^{chip/chip}$ or *Dnmt1*$^{+/+}$ mice, although substantially less so than the DNA from *Dnmt1*$^{-/-}$ null ES cells. Mice carrying the different *Dnmt1* alleles were obtained at the expected Mendelian ratios, indicating that reduction of Dnmt1 expression to 10% was compatible with viability. However, compound heterozygotes (*Dnmt1*$^{chip/-}$) were runted and their weight at birth was only 70% that of *Dnmt1*$^{+/-}$ mice, in contrast to mice homozygous for the hypomorphic allele (*Dnmt1*$^{chip/chip}$), which were normal in size (Fig. 2A). *Dnmt1*$^{chip/-}$ mice, although remaining substantially underweight, were fertile and generated litters of nonrunted pups when bred with wild-type mice.

In addition to the runted phenotype, 80% of *Dnmt1*$^{chip/-}$ mice developed aggressive thymic tumors at 4 to 8 months of age. Cumulative survival of the *Dnmt1*$^{chip/-}$ mice is shown in Fig. 2B. Histological analysis classified the tumors as T cell lymphomas (*11*), and fluorescence-activated cell sorting (FACS) analysis revealed that most tumors were CD4$^-$/CD8$^+$ or CD4$^+$/CD8$^+$ (Fig. 2D). When tested for D-to-J rearrangements in the T cell receptor β locus, four of 10 tumors showed a predominant Dβ1-to-Jβ1 rearranged band (Fig. 2C, lanes 5, 9, 11, and 13) consistent with monoclonality. Tumors without Dβ1-to-Jβ1 recombination may have rearranged other D and J elements. Monoclonality suggests that hypomethylation induces cancer in a precursor cell, with subsequent events leading to malignant tumor formation. Consistent with frequent activation of the c-*myc* oncogene in mouse and human lymphoma (*12*), we found that c-*myc* was overexpressed in almost all hypomethylated tumors (15/18 *Dnmt1*$^{chip/-}$, Fig. 3C).

Genomic hypomethylation may contribute to lymphomagenesis by an epigenetic or a genetic mechanism. We considered three possible mechanisms.

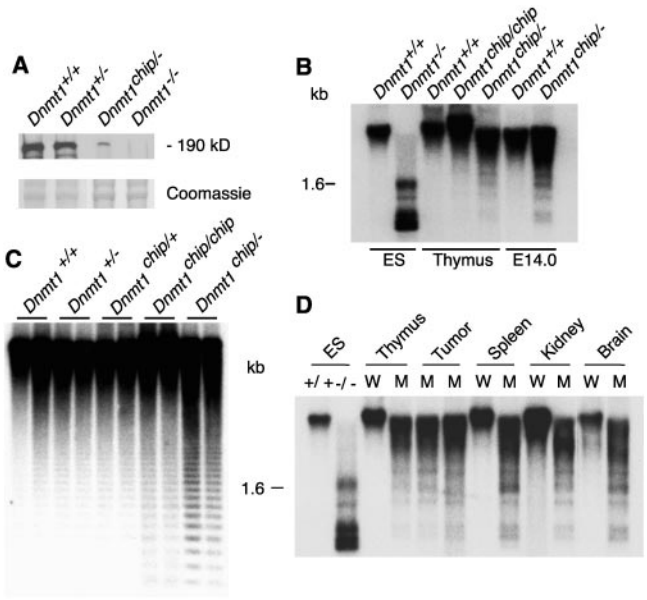

Fig. 1. Genomic hypomethylation in *Dnmt1* hypomorphic mice. (**A**) Immunoblot analysis of protein extracts from ES cells, using a C-terminal Dnmt1 chicken antibody (*34*). The level of Dnmt1 in *Dnmt1*$^{chip/-}$ ES cells was markedly reduced, demonstrating the hypomorphic nature of this allele. The *Dnmt1*$^{-/-}$ negative control extracts did not show any bands, as expected [c allele (*7*)]. A Promega antibody to chicken immunoglobulin Y (IgY), with horseradish peroxidase as secondary antibody, was used; detection was performed with the Amersham Pharmacia Biotech ECL kit. The Coomassie gel shows total protein levels in each sample. (**B**) Southern blot of methylation status of IAPs in *Dnmt1*$^{chip/chip}$ and *Dnmt1*$^{chip/-}$ mice. Genomic DNA was digested with the methylation-sensitive restriction enzyme Hpa II and probed with an IAP cDNA probe (*10*). Hypomethylation was detected in thymus from 6-week-old *Dnmt1*$^{chip/-}$ mice and in *Dnmt1*$^{chip/-}$ embryonic day (E) 14.0 fibroblasts but not in *Dnmt1*$^{chip/chip}$ homozygotes or wild-type controls, as evidenced by the presence of lower molecular weight DNA fragments. (**C**) Southern blot analysis of centromeric repeat methylation of E14.0 fibroblasts from mice containing various *Dnmt1* alleles. Hypomethylation is evident in the *Dnmt1*$^{chip/-}$ lanes. (**D**) Southern blot analysis of IAP methylation status in tissues from a 6-week-old *Dnmt1*$^{chip/-}$ mouse and in lymphomas. Significant hypomethylation is evident in all *Dnmt1*$^{chip/-}$ tissues. Controls for methylation (*Dnmt1*$^{+/+}$ ES cells) and hypomethylation (*Dnmt1*$^{-/-}$ ES cells) are also shown (ES, ES cells; W, *Dnmt1*$^{+/+}$; M, *Dnmt1*$^{chip/-}$).

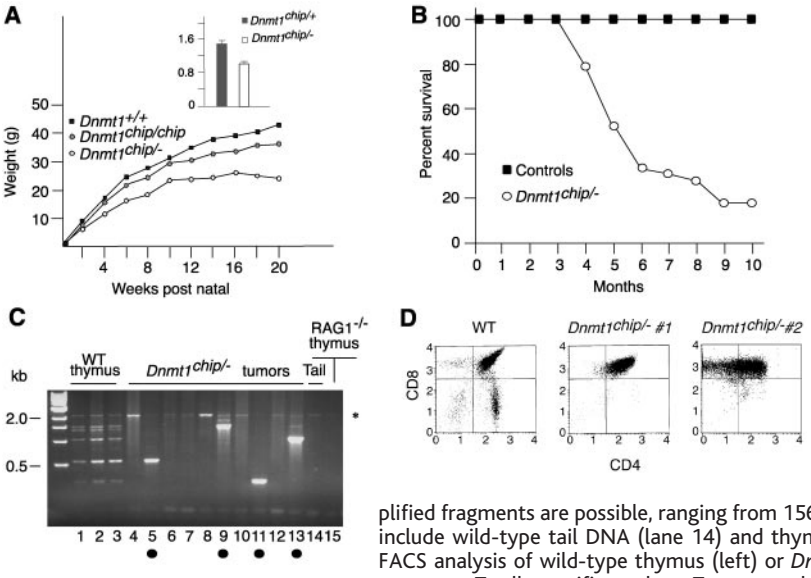

Fig. 2. *Dnmt1* hypomorphs are runted and develop T cell lymphomas. (**A**) Average weight of *Dnmt1*$^{chip/+}$ (n = 20) and *Dnmt1*$^{chip/-}$ (n = 20) male littermates at birth (inset). *Dnmt1*$^{chip/-}$ mice were 66% as large as *Dnmt1*$^{chip/+}$ mice. Females showed the same runt phenotype. The error bar indicates ±1 SD, $p < 0.0001$ (Student t test, StatView 5.0.1 software). Also shown are growth curves of *Dnmt1*$^{chip/chip}$, *Dnmt1*$^{chip/-}$, and wild-type male mice. Six to 10 mice of each genotype were used for each data point. (**B**) Cumulative survival of *Dnmt1*$^{chip/-}$ mice. Most *Dnmt1*$^{chip/-}$ mice became terminally ill between 4 and 8 months of age. Control mice were *Dnmt1*$^{chip/chip}$ (n = 18); experimental mice were *Dnmt1*$^{chip/-}$ (n = 33). Mice were autopsied when visibly ill. At autopsy, 23 of 33 *Dnmt1*$^{chip/-}$ mice had developed tumors (21 lymphomas and 2 fibrosarcomas). Autopsy of *Dnmt1*$^{chip/chip}$ mice at 6 months (n = 12) and 12 months (n = 6) showed no evidence of tumor formation. (**C**) Dβ1-to-Jβ1 rearrangement at the TCRβ locus was analyzed by the polymerase chain reaction as described (*35*), using primers 1 and 4 therein. The asterisk denotes the germline configuration [2171 base pairs (bp)]. When rearranged, five different amplified fragments are possible, ranging from 1561 to 381 bp (see wild-type thymus, lanes 1 to 3). Controls also include wild-type tail DNA (lane 14) and thymus DNA from a recombination-deficient RAG1$^{-/-}$ mouse. (**D**) FACS analysis of wild-type thymus (left) or *Dnmt1*$^{chip/-}$ tumors (middle and right) stained for CD4 and CD8 receptors, T cell–specific markers. Tumors analyzed (n = 16) contained either double-positive CD4^{high}/CD8^{high} cells (9/16, middle panel) or CD4^{low}/CD8^{high} cells (7/16, right panel).

(i) Hypomethylation may induce endogenous retroviral elements, leading in turn to insertional activation of proto-oncogenes (*13*). To test this idea, we hybridized RNA from randomly selected tumors with a Moloney murine leukemia virus (MMLV) cDNA probe and an IAP probe to detect endogenous retroviral and IAP expression, respectively. Of nine *Dnmt1*$^{chip/-}$ tumors, none showed C-type retroviral activation (Fig. 3A) (*14*) and only one of eight tumors showed a moderate increase in IAP expression (Fig. 3B, lane 7). In contrast, strong C-type retroviral expression was seen in a MMLV-induced lymphoma [Fig. 3A, slot a1 (*15*)] and IAP expression was highly activated in *Dnmt1*$^{-/-}$ fibroblasts [Fig. 3B, lanes 10 to 12 (*16*)]. Because c-*myc* is a frequent target for insertional activation by retroviral elements (*17*), we searched for inserted proviral elements in hypomethylated and MMLV-induced tumors. In 3 of 12 MMLV-induced tumors, an insertional rearrangement was seen in the vicinity of the c-*myc* locus, in agreement with previous observations (*17*). In contrast, no rearrangements were detected in hypomethylated tumors [0/18 (*11*)]. We conclude that the extent of hypomethylation in *Dnmt1*$^{chip/-}$ mice does not effectively activate endogenous retroviral elements and that virus insertions may not be a prevalent mechanism in hypomethylation-induced lymphoma.

(ii) Hypomethylation may activate proto-oncogenes through epigenetic effects (*18, 19*). Indeed, c-*myc* was overexpressed in most hypomethylated tumors (Fig. 3C). However, it is unlikely that activation of c-*myc* is a direct consequence of promoter demethylation because the gene is expressed at normal levels in thymuses from 2- and 4-week-old mice that show a level of hypomethylation identical to that of the tumors [Fig. 1D (*11*)]. In addition, c-*myc* was not activated in *Dnmt*$^{-/-}$ fibroblasts that are almost completely demethylated (*16*). Finally, if oncogene activation by hypomethylation stimulated T cell proliferation as a first step in transformation, one would expect the lymphomas to be polyclonal rather than monoclonal (Fig. 2C).

(iii) Hypomethylation may induce genomic instability. In fact, a significantly increased frequency of chromosomal rearrangements such as loss of heterozygosity (LOH) was observed in *Dnmt1* mutant ES cells, suggesting that normal levels of methylation are important for genomic stability (*20*). Defects in DNA methylation have been linked to genome instability in studies of colorectal tumor cell lines (*21*), mouse tumor models (*22, 23*), and patients with immunodeficiency–centromeric instability–facial anomalies (ICF) syndrome (*24, 25*).

To test whether DNA hypomethylation increases genomic instability in *Dnmt1*$^{chip/-}$ tumors, we performed array-based comparative genome hybridization [array CGH (*26*)] using thymic tumor genomic DNA prepared from *Dnmt1*$^{chip/-}$ and Mov-1 (*15*) and Mov-14 (*27*) MMLV transgenic mice (Fig. 3D). There was a statistically significant difference in chromosome gains between these tumor classes (Table 1). Ten of 12 hypomethylated tumors exhibited a gain of chromosome 15, whereas only 2 of 12 MMLV-induced tumors showed this change ($P = 0.004$). Relative to MMLV-induced tumors, hypomethylated tumors also displayed a gain of chromosome 14 (4/12 versus 0/12, $P = 0.05$) and a higher degree of duplicated and deleted chromosome regions (Table 1) (Fig. 3D).

Together with the centromeric hypomethylation we observed (Fig. 1C), these results suggest a causal link between DNA hypomethylation and chromosomal instability as one mechanism leading to tumorigenesis. The increased fluorescence ratios observed for chromosomes 14 and 15 are consistent with single-copy whole-chromosome gains throughout the tumor (Fig. 3D), which suggests that they are early events in the development of these monoclonal T cell lymphomas. Chromosome 15 is frequently duplicated in mouse T cell tumors (*28, 29*) and contains the oncogene c-*myc*, which when overexpressed causes T cell lymphomas (*17*). The fact that c-*myc* is overex-

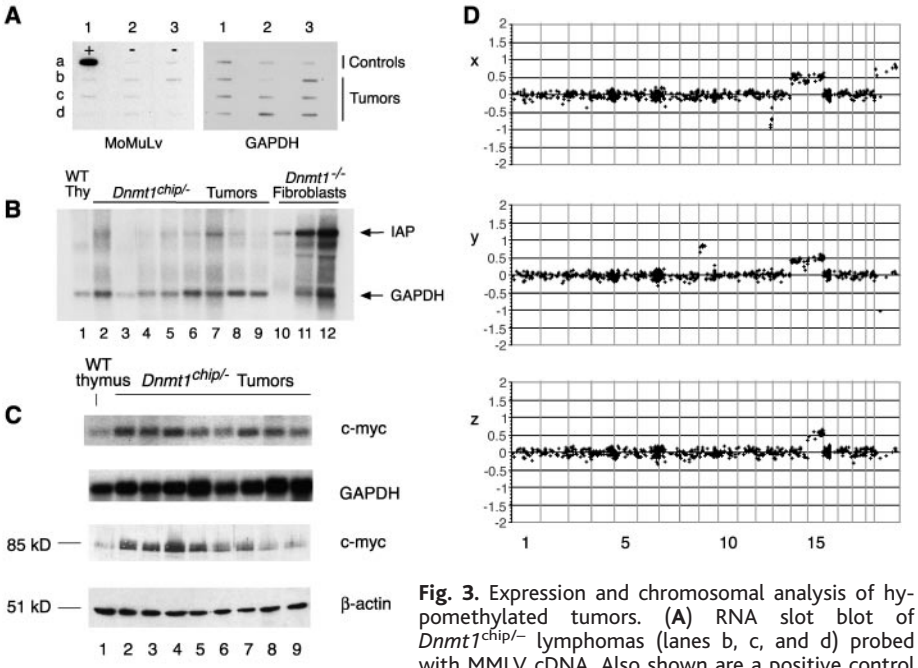

Fig. 3. Expression and chromosomal analysis of hypomethylated tumors. (**A**) RNA slot blot of *Dnmt1*$^{chip/-}$ lymphomas (lanes b, c, and d) probed with MMLV cDNA. Also shown are a positive control lymphoma from a Mov-1 mouse [slot a1 (*15*)] and negative control thymuses from wild-type 129/Sv (slot a2) and a wild-type littermate of a tumor-bearing mouse (slot a3). (**B**) Northern blot of IAPs in *Dnmt1*$^{chip/-}$ tumors. IAPs can be detected in most tumors, whereas wild-type thymus does not show IAP expression. Positive control (lanes 10 to 12, 1:3 serial dilutions) are *Dnmt1*$^{-/-}$ hypomethylated fibroblasts that have been shown to activate IAP expression (*16*). Comparison of IAP and glyceraldehyde-3-phosphate dehydrogenase (GAPDH) levels shows that most clones express much less IAPs than the positive control. (**C**) Expression levels of c-*myc* were assessed by Northern blot (top two panels) and by immunoblot (bottom two panels). Lanes 2 to 7 are tumors that showed chromosome 15 trisomy; lanes 8 and 9 are tumors that are diploid for chromosome 15. Probes used were c-*myc* exon 2 for the Northern analysis and a rabbit polyclonal IgG antibody to c-*myc* for immunoblots (Santa Cruz Biotechnology). (**D**) Array comparative genome hybridization (CGH) analyses of three *Dnmt1*$^{chip/-}$ tumors, showing clear single-copy, whole-chromosome gain of chromosome 15 (x, y, and z), whole-chromosome gains of 14 and loss on distal 12 (x), and gains of chromosome 14 and proximal 9 (y). The X gain (x) reflects a sex difference between tumor and control. Array CGH was performed as in (*26*). Fluorescence ratios (average of quadruplicate measurements) for each bacterial artificial chromosome are plotted as a function of genome location based on the February 2002 freeze of the assembled mouse genome sequence (http://genome.ucsc.edu). Vertical lines delimit chromosome boundaries.

Table 1. Gains or losses of chromosomes in *Dnmt1*$^{chip/-}$ and MMLV-induced tumors. The numbers indicate the number of times a particular event occurred in the *Dnmt1*$^{chip/-}$ or Moloney tumors. These events were not mutually exclusive; many tumors exhibited multiple chromosomal events.

Chromosomal changes	*Dnmt1*$^{chip/-}$ tumors ($n = 12$)	MMLV-induced tumors ($n = 12$)
Chr 15 gain	10	2
Chr 14 gain	4	0
Chr 10 gain	0	1
Partial Chr 9 gain	2	0
Partial Chr 4 gain	1	0
Partial Chr 16 loss	1	0
Partial Chr 12 loss	1	0

pressed (RNA and protein) in most hypomethylated tumors (Fig. 3C) is consistent with a mechanism in which a gain of chromosome 15 contributes, at least in part, to the elevated expression of c-*myc*. Moreover, c-*myc* expression was lower in the two tumors that did not show trisomy 15 than in the other tumors (Fig. 3C).

Our results show that genomic hypomethylation causes tumorigenesis in mice and is associated with the acquisition of additional genomic changes. Consistent with this, genomic hypomethylation was found to promote tumorigenesis in a different mouse tumor model and to increase the rate of LOH in cultured fibroblasts (*23*). However, it remains possible that DNA hypomethylation contributes to tumorigenesis through other mechanisms unrelated to chromosomal instability. The phenotype of hypomethylated mice is also consistent with that of *Suv39h* histone methyltransferase mutant mice; hence, DNA and histone methylation, pericentric chromatin structure, and the maintenance of chromosomal stability may be linked (*30*).

DNA methyltransferase inhibitors such as 5-aza-2′-deoxycytidine have been used successfully to treat cancer in humans (*19, 31*) and mice (*32, 33*). The efficacy of these drugs is presumably due to their ability to reverse the epigenetic silencing of tumor suppressor genes. In light of our results, however, this therapeutic strategy should perhaps be considered a double-edged sword: Genomic demethylation may protect against some cancers such as intestinal tumors in the Apc^{Min} mouse model (*32*) but may promote genomic instability and LOH (*20, 23*) and increase the risk of cancer in other tissues, as seen in hypomethylated mutant mice.

References and Notes

1. P. A. Jones, S. B. Baylin, *Nature Rev. Genet.* **3**, 415 (2002).
2. A. P. Feinberg, B. Vogelstein, *Nature* **301**, 89 (1983).
3. M. Ehrlich, *Oncogene* **21**, 5400 (2002).
4. M. A. Gama-Sosa, *Nucleic Acids Res.* **11**, 6883 (1983).
5. J. N. Lapeyre, F. F. Becker, *Biochem. Biophys. Res. Commun.* **87**, 698 (1979).
6. R. Jaenisch, A. Bird, *Nature Genet.* **33** (suppl.), 245 (2003).
7. H. Lei *et al.*, *Development* **122**, 3195 (1996).
8. E. Li, T. H. Bestor, R. Jaenisch, *Cell* **69**, 915 (1992).
9. K. L. Tucker *et al.*, *Genes Dev.* **10**, 1008 (1996).
10. C. P. Walsh, J. R. Chaillet, T. H. Bestor, *Nature Genet.* **20**, 116 (1998).
11. F. Gaudet, A. Eden, R. Jaenisch, unpublished data.
12. S. Cory, D. L. Vaux, A. Strasser, A. W. Harris, J. M. Adams, *Cancer Res.* **59** (suppl.), 1685s (1999).
13. R. Jaenisch, A. Schnieke, K. Harbers, *Proc. Natl. Acad. Sci. U.S.A.* **82**, 1451 (1985).
14. R. Jaenisch, *Proc. Natl. Acad. Sci. U.S.A.* **73**, 1260 (1976).
15. D. Jahner, R. Jaenisch, *Nature* **287**, 456 (1980).
16. L. Jackson-Grusby *et al.*, *Nature Genet.* **27**, 31 (2001).
17. G. Selten, H. T. Cuypers, M. Zijlstra, C. Melief, A. Berns, *EMBO J.* **3**, 3215 (1984).
18. E. Wainfan, L. A. Poirier, *Cancer Res.* **52**, 2071s (1992).
19. A. R. Karpf, D. A. Jones, *Oncogene* **21**, 5496 (2002).
20. R. Z. Chen, U. Pettersson, C. Beard, L. Jackson-Grusby, R. Jaenisch, *Nature* **395**, 89 (1998).
21. C. Lengauer, K. W. Kinzler, B. Vogelstein, *Proc. Natl. Acad. Sci. U.S.A.* **94**, 2545 (1997).
22. B. N. Trinh, T. I. Long, A. E. Nickel, D. Shibata, P. W. Laird, *Mol. Cell. Biol.* **22**, 2906 (2002).
23. A. Eden, F. Gaudet, A. Waghmare, R. Jaenisch, *Science* **300**, 455 (2003).
24. M. Jeanpierre *et al.*, *Hum. Mol. Genet.* **2**, 731 (1993).
25. G. L. Xu *et al.*, *Nature* **402**, 187 (1999).
26. G. Hodgson *et al.*, *Nature Genet.* **29**, 459 (2001).
27. C. Stewart, K. Harbers, D. Jahner, R. Jaenisch, *Science* **221**, 760 (1983).
28. Z. Wirschubsky, P. Tsichlis, G. Klein, J. Sumegi, *Int. J. Cancer* **38**, 739 (1986).
29. M. Muto, Y. Chen, E. Kubo, K. Mita, *Jpn. J. Cancer Res.* **87**, 247 (1996).
30. A. H. F. M. Peters *et al.*, *Cell* **107**, 323 (2001).
31. V. Zagonel *et al.*, *Leukemia* **7** (suppl. 1), 30 (1993).
32. P. W. Laird *et al.*, *Cell* **81**, 197 (1995).
33. A. R. MacLeod, M. Szyf, *J. Biol. Chem.* **270**, 8037 (1995).
34. F. Gaudet, D. Talbot, H. Leonhardt, R. Jaenisch, *J. Biol. Chem.* **273**, 32725 (1998).
35. C. E. Whitehurst, S. Chattopadhyay, J. Chen, *Immunity* **10**, 313 (1999).

36. We thank R. Flannery for help with the mouse colony, and K. Hong and C. Cardoso for helpful discussions. Supported by grants from the Max Delbrück Center and the Deutsche Forschungsgemeinschaft (H.L.), by NIH grant CA87869 (R.J.), and by EMBO fellowship ALTF 43-1999 and Boehringer Ingelheim (A.E.).

18 February 2003; accepted 10 March 2003

Regulation of Elongating RNA Polymerase II by Forkhead Transcription Factors in Yeast

Antonin Morillon,[1] Justin O'Sullivan,[2] Abul Azad,[2] Nicholas Proudfoot,[2] Jane Mellor[1]*

The elongation phase of transcription by RNA polymerase II (RNAPII) is highly regulated and tightly linked to pre–messenger RNA (pre-mRNA) processing. Recent studies have implicated an early elongation checkpoint that facilitates the link to pre-mRNA processing. Here we show that the yeast forkhead transcription factors, Fkh1p and Fkh2p, associate with the coding regions of active genes and influence, in opposing ways, transcriptional elongation and termination. These events are coordinated with serine-5 and -2 phosphorylation of the heptad repeat of the carboxy-terminal domain (CTD) of RNAPII. Our results suggest that, in addition to their documented promoter function, Fkh1p and Fkh2p coordinate early transcription elongation and pre-mRNA processing. This may reflect a general feature of gene regulation in eukaryotes.

The winged-helix forkhead (Fkh) family of transcription factors is highly conserved in eukaryotes with roles in cell cycle control, cell death, proliferative responses, and differentiation (*1*). In yeast, *FKH1* and *FKH2* influence expression of a wide range of genes (*2*), including those that control the G_2–M phase transition of the cell cycle (*3*, *4*). Activation of genes of the *CLB2* cluster, expressed at G_2–M phase, requires cooperative binding of the Fkh2p and the Mcm1p transcription factors to the Swi Five Factor (SFF) site in the promoter. Fkh2p is the preferred component of the SFF factor, although Fkh1p substitutes in the absence of Fkh2p (*5*) and either factor is sufficient for activator recruitment (*4*). Previous studies have shown that the effects of ablation of each individual Fkh factor on the steady-state levels of *CLB2* mRNA are different; Fkh1p is required to repress expression, whereas Fkh2p activates expression to normal levels (*6*–*8*). This suggests additional opposing functions for Fkh factors in regulating *CLB2* expression. Structural and functional studies reveal a linker histone-like structure for the winged-helix Fkh domain and suggest interactions with chromatin other than sequence-specific DNA binding (*9*, *10*). In agreement with a more general effect on gene expression, our results demonstrate that Fkh factors differentially regulate the elongation phase of transcription at *CLB2* and at other loci.

We have analyzed the binding of Fkh factors to *CLB2* with the use of chromatin immunoprecipitation (ChIP) in strains expressing epitope-tagged Fkh factors (*11*). As expected, Fkh2p binds strongly and Fkh1p weakly to the upstream activating sequence (UAS) region on the promoter (*5*) (Fig. 1B). The majority of Fkh1p is associated with the first 600 base pairs (bp) of the transcribed region, whereas, in addition to UAS binding, a second peak of Fkh2p is present at the beginning of the coding region, extending toward the 3′ end of the gene. The unexpected presence of Fkh1p and Fkh2p in the *CLB2* coding region suggests a role in transcriptional elongation, in addition to their well-known function in *CLB2* activation involving UAS association.

We investigated the distribution of RNAPII over the *CLB2* gene (Fig. 1C; fig. S1). In wild-type (WT), the distribution of RNAPII (Rbp3-

[1]Department of Biochemistry, University of Oxford, South Parks Road, Oxford OX1 3QU, UK. [2]Sir William Dunn School of Pathology, University of Oxford, South Parks Road, Oxford OX1 3RE, UK.

*To whom correspondence should be addressed. E-mail: emellor@molbiol.ox.ac.uk